Double ionization of helium by electron impact in the impulsive regime

A. Dorn,[1] A. Kheifets,[2] C. D. Schröter,[1] B. Najjari,[1] C. Höhr,[1] R. Moshammer,[1] and J. Ullrich[1]

[1]*Max-Planck-Institut für Kernphysik, Saupfercheckweg 1, 69117 Heidelberg, Germany*

[2]*Research School for Physical Sciences and Engineering, Australian National University,*

Canberra, Australian Capital Territory 0200, Australia

The dynamics of helium double ionization by 2 keV electron impact has been investigated experimentally and theoretically at large momentum transfer of $|\mathbf{q}|=2$ a.u. Fully resolved fivefold differential cross sections (FDCS's) are presented for symmetric and asymmetric energy sharing between the two ejected electrons at excess energies from 10 to 40 eV, and for the coplanar as well as the out-of-plane scattering geometries. Experimentally, a multielectron–recoil-ion coincidence technique has been applied and a large part of the final-state momentum space has been mapped. The presently employed theoretical model treats the interaction between the two slow ejected electrons nonperturbatively using the convergent close-coupling method, whereas the projectile-target interaction is described in the first Born approximation. The experimental and theoretical FDCS's agree well in shape. The cross section is dominated by two pairs of strong peaks. From this pattern it can be concluded that the two-step 1 mechanism, which is due to interelectron interaction after a single ionizing collision, is the dominant ionization process for the present kinematics.

I. INTRODUCTION

The investigation of electron-impact ionization has contributed considerably to our understanding of the correlated fragmentation dynamics of atomic systems. Until recently, most of the research performed in this field dealt with single ionization. This work was initiated by Ehrhardt and collaborators [1,2] who first realized kinematically complete (e,2e) experiments in which the momentum vectors of all continuum particles were under full control. These experiments gave rise to a rapid development of the field. As a consequence, a profound understanding of the electron-impact single ionization of atoms has been gained [3]. The most basic collision processes like electron-impact ionization of hydrogen can now be calculated numerically with high precision [4].

The next step toward more "complex" few-body systems with more than two electrons in the final continuum state is an investigation of electron-impact double ionization of atoms. In comparison to single ionization, several challenging aspects arise. First, the initial state of the simplest possible target, helium, already represents a highly correlated system. In principle, its binding energy can be calculated numerically to an arbitrary accuracy. However, the ground-state correlations can be incorporated into the calculations of double ionization to only a limited degree of complexity. Furthermore, details of the dynamics are expected to depend sensitively on specific features of the correlated ground-state wave function, and there is no guarantee that even complicated wave functions, optimized to minimize the binding energy, would produce a correct two-electron ionization amplitude. Secondly, depending on the projectile velocity, the ionization process can go beyond the first order in the projectile-target interaction and higher-order interactions may contribute significantly. If the target-electron correlation is neglected, double ionization is possible only through higher-order collisions. Second-order matrix elements as well as their interference with the first-order contributions have not yet been consistently included in theoretical models. One usually tries to identify the most important reaction mechanisms and to include the corresponding matrix elements. Thirdly, a major challenge to theory is to describe the final state with four interacting particles in the continuum. There are approximate correlated three-particle continuum wave functions that have been worked out for (e,2e) and (γ,2e) [5,6] (for a review see [7]), some of which have been extended to the four-particle continuum [8–10].

The easiest way to tackle these problems is to consider double ionization by fast electron impact at an incident energy of several keV and small momentum transfer. Under these conditions the projectile-target interaction can be treated in a good approximation to the first order. It is this regime where most existing calculations have been performed [11,12]. Only a little work has been reported where higher-order interactions were included by applying the second Born approximation [13] or by employing explicit four-body wave functions [8,9].

Experimentally, serious obstacles have also to be overcome. The most stringent test for theory is provided by kinematically complete experiments in which the energies and angles of all participating particles are determined and therefore fully differential cross sections are obtained. In the case of particle-impact-induced double ionization, the final-state four-particle momentum space spans 12 dimensions, of which eight are independent. Therefore, at least three particles have to be detected in coincidence. Furthermore, the total cross section for double ionization is very small, only of the order of 10^{-2} or less of the corresponding single-ionization cross section. The first (e,3e) experiment was performed 12 years ago by Lahmam-Bennani and co-workers [14] on argon using conventional electron spectroscopy techniques. The subsequent development of devices that were able to detect a certain angular range simultaneously allowed absolute cross sections to be obtained with sufficient statistics for a more quantitative comparison with theory [15,16].
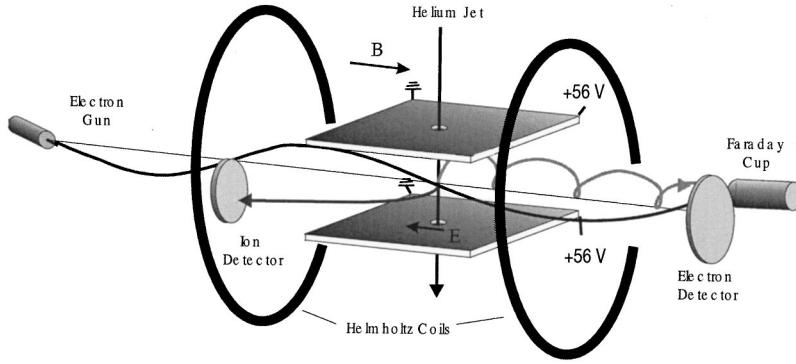
FIG. 1. Schematic view of the "reaction microscope."

Nevertheless, for the fundamental helium target, experiments employing conventional electron spectroscopy techniques are restricted to particular cases with relatively large cross sections, such as the dipole limit of a small momentum transfer [10,12,17]. For larger momentum transfer of several atomic units conventional experiments are feasible only for heavier quasi-two-electron targets like magnesium [18].

In order to overcome these limitations we apply in the present work a multielectron–recoil-ion coincidence technique which has already been demonstrated to enable $(e,3e)$ experiments on helium [19]. A 2 keV electron impact is considered and the fully differential cross sections are obtained over the full final-state momentum space. The kinematics of the reaction covers a range of momentum transfer from the optical limit to high values up to 5 a.u., and a large range of relative emission angles and energy partitions of two slowly ejected electrons $(E_{b,c} < 30$ eV$)$. The results for small momentum transfer have been discussed previously [20]. In this work the dynamics of double ionization is studied for impulsive collisions with relatively large momentum transfer of $|\mathbf{q}| = 2$ a.u.

The rest of the paper is organized as follows. In Sec. II the experimental apparatus is described. In Sec. III the experimental results are presented and compared with convergent close-coupling (CCC) calculations for different energies of the ejected electrons and for the in-plane and out-of-plane geometries. Finally, we give a summary in Sec. IV.

II. EXPERIMENT

The experiments were performed with a version of our multielectron recoil-ion momentum spectrometer ("reaction microscope") that is designed to fit the particular requirements of electron-scattering experiments. The momentum vectors of two slowly ejected electrons $\mathbf{k}_b$ and $\mathbf{k}_c$ and the momentum vector of the recoiling ion $\mathbf{k}_{He2+}$ emitted in an $(e,3e)$ reaction are measured in coincidence. Therefore nine momentum components, one more than necessary to completely fix the kinematics, are obtained. Applying momentum conservation, the momentum $\mathbf{k}_a$ of the fast scattered electron or, equivalently, the momentum $\mathbf{q}$ transferred by the scattered projectile is determined:

$$\mathbf{q} = \mathbf{k}_0 - \mathbf{k}_a = \mathbf{k}_b + \mathbf{k}_c + \mathbf{k}_{\text{ion}}. \tag{1}$$

Here $\mathbf{k}_0$ is the momentum of the incoming projectile. The redundant information obtained experimentally can be used to discriminate against accidental coincidences by examining for each double ionization event whether energy conservation is fulfilled:

$$E_0 = E_a + E_b + E_c + E_{\text{bind}}.$$

Here E_{bind} is the double-ionization potential.

Since a detailed description of the working principle of the reaction microscope has been reported earlier [21], we give here only a brief outline stressing the particularities of the present setup. A scheme of the apparatus is presented in Fig. 1. A conventional electron gun was used to produce a pulsed primary beam with a repetition rate of 500 kHz and a pulse length of $\Delta t \approx 1$ ns. The helium target was prepared in a precooled triple-stage supersonic jet. The helium gas expanded through a 30 μm aperture which was cooled to liquid-nitrogen temperature to form a well-localized (2.0 mm diameter) and dense (10^{11} atoms/cm^3) target at the intersection point with the electron beam. Ions and low-energy electrons produced in $(e,3e)$ collisions were extracted to opposite directions by a uniform 2.7 V/cm electric field applied along the apparatus axis and were detected by two-dimensional position-sensitive multichannel plates. The extraction field was produced by a voltage gradient along two ceramic plates with resistive coating above and below the scattering region. A solenoidal magnetic field of 12 Gauss produced by a pair of Helmholtz coils forces the slow electrons with nonzero transverse momentum components into spiral trajectories. In this way electrons with energies below 30 eV and essentially all ions are detected with the full solid angle of 4π. From the times of flight (TOF's) and the measured positions on the detectors the trajectories of the particles can be reconstructed and their initial longitudinal and transverse momentum components are obtained. For electrons the calculation of the initial transverse momentum is not unambiguous if their TOF is an integer number of cyclotron revolutions (for details, see Ref. [21]). In the present experiment the cross section for the corresponding longitudinal momentum vectors was obtained by a second experimental run applying a slightly different electric extraction field and therefore changing the TOF of the electrons. The 80 mm active diameter electron detector is equipped with a fast delay-line readout and a multihit time-to-digital converter. Thus, positions as well as arrival times of both elec-

trons emitted in a double-ionization event are determined if their flight-time difference exceeds the detectors dead time of about 15 ns. This results in a small loss of momentum space in the final state for electrons having similar momenta in the longitudinal direction toward the electron detector.

The electron and ion momentum resolution of the spectrometer depends mainly on the size of the interaction volume and the magnitude of the electric and magnetic extraction fields applied. The ion momentum resolution additionally relies on the temperature of the target gas. The effect of the longitudinal extension of the interaction volume on the TOF is eliminated by a time-focusing arrangement in which the lengths of the acceleration region and a drift region are matched. Therefore it is favorable to align the projectile beam along the longitudinal direction. In this way it is possible to combine a relatively large length of the interaction volume (2 mm) and thus high signal intensity with still good resolution for the longitudinal momentum components. The transverse extension of the interaction volume is minimized by focusing the projectile beam into the target using the solenoidal magnetic field. The electron gun, ion detector, helium target, and electron detector are equally spaced at a distance of 33 cm from each other. Except for the ion detector, they are aligned on the axis of the apparatus, which coincides with the axis of the magnetic field. The TOF of the primary electrons ($E_0 = 2$ keV) from the gun to the target interaction point is equal to the electron cyclotron revolution time in the magnetic field ($t_c = 26$ ns). Therefore the magnetic-lens effect images an electron-beam focus at the exit of the electron gun into the helium jet where the beam diameter is below 0.5 mm. The superimposed initial transverse momentum component results in an offset of 7 cm of the electron beam from the apparatus axis at the position of the ion detector (flight time $t_c/2$) and at the position of the electron detector (flight time $3t_c/2$). In this way the projectile beam passes both detectors and is deposited in a Faraday cup next to the electron detector. The momentum resolution with the present extraction fields is about $|\Delta k_c| \approx 0.05$ a.u. for electrons and $|\Delta k_{He}| \approx 0.3$ a.u. for the doubly charged helium ions. The resulting angular resolution for electrons is about $\pm 5°$ for 5 eV electrons.

III. RESULTS

Experimentally, the square of the four-particle momentum wave function in the final-state continuum is obtained from which differential cross sections can be extracted, in principle, for arbitrary coordinates which seem to be appropriate to study the process. Here we present cross sections $d^5\sigma/d\Omega_a d\Omega_b d\Omega_c dE_b dE_c$ differential with respect to the energies $E_{b,c}$ and solid angles $\Omega_{b,c}$ of the two slowly ejected electrons and in the solid angle Ω_a of the fast emitted electron.

Under the present conditions of a fast projectile ($E_0 = 2$ keV) and two slow final-state electrons ($E_{b,c} < 30$ eV), exchange processes can be neglected. Therefore the fast outgoing electron can be identified with the scattered projectile, and by fixing the scattering angle the amount of momentum

$|\mathbf{q}|$ transferred to the target is determined. In the following the cross sections are presented in the angle scanning mode: for a given momentum transfer and for fixed energies of the ejected electrons the cross section is plotted as a function of the ejected-electron emission angles. Thus a direct comparison with data obtained by conventional electrostatic electron spectrometers is possible. In this work we investigate collisions with fairly large momentum transfer of $|\mathbf{q}| = 2 \pm 0.4$ a.u., far from the optical limit. The question arises of how the double-ionization dynamics can be characterized under this condition. From ($e,2e$) studies at high momentum transfer it is known that single ionization can be very well described as a binary knock-out collision of the projectile with a target electron. The cross section peaks for the so-called Bethe kinematics where the residual ion does not take part in the collision and carries away only a small momentum. The ionized electron is emitted into the direction of the momentum transfer. In the case of double ionization, different reaction mechanisms and corresponding matrix elements are usually considered: the shake-off, the two-step 1 (TS1), and the two-step 2 (TS2) processes [22,23]. In the shake-off process only one target electron takes momentum in a direct ionizing collision with the projectile and is emitted into the direction of $\mathbf{q}$. The second electron is "shaken" into the continuum, i.e., it is emitted due to the subsequent relaxation of the singly charged ionic core. From first principles, it should not be emitted into a particular direction and furthermore is expected at a low energy since its momentum originates from the Compton profile of the initial atomic ground state. The recoiling ion balances the momentum of the shake-off electron.

In the TS1 process the incident electron strikes a target electron which in turn ionizes the second electron in a binary collision on its way out of the atom. The residual ion should have a small recoil momentum. In the limit of high energy of the two ejected electrons their relative angle should be 90°.

Both these processes are of the first order in the projectile-target interaction and show axial symmetry with respect to $\mathbf{q}$. In contrast, the TS2 is a second-order process in which the projectile interacts and ionizes each target electron sequentially. A signature of second- or higher-order processes is a breakup of the symmetry of the cross section with respect to $\mathbf{q}$. One has to bear in mind the following complications. The "mechanisms" discussed above are quantum-mechanical matrix elements which interfere if several amplitudes contribute with similar magnitudes to the same point in the final-state momentum space. Furthermore, the strict directions that are expected for ejected electrons with high energies are modified for lower energies as in the present experiment since the electron-electron repulsion in the continuum increases their relative angle and the momentum distribution in the initial target ground state smears out the cross-section maxima.

We first investigate the cross section for coplanar scattering geometry which is illustrated in Fig. 2. Here both target electrons are ejected in the scattering plane defined by the incoming and scattered projectile. In Fig. 3(a) the data for
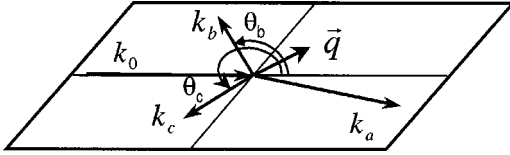
FIG. 2. Coplanar scattering geometry. Both ejected electrons with momenta $\mathbf{k}_b$ and $\mathbf{k}_c$ move in the plane defined by the incoming and scattered projectile with momenta $\mathbf{k}_0$ and $\mathbf{k}_a$, respectively. The momentum transfer is defined as $\mathbf{q}=\mathbf{k}_0-\mathbf{k}_a$.

symmetric energy sharing $E_b=E_c=5$ eV are presented in a density plot which allows us to show the cross section for the full angular range of θ_b and θ_c and to visualize the overall structure of the cross section with nodal lines and inherent symmetries. The angular range that is not affected by the electron detector dead time is inside the circular solid lines. The cross-section pattern consists of four maxima of which the two in the lower right part are equivalent to those in the upper left part. Since for equal energy sharing $E_b=E_c$ both electrons are interchangeable the cross section is symmetric with respect to the diagonal line $\theta_b=\theta_c$.

A similar four-maximum cross section is observed in the $(\gamma,2e)$ reaction [24] and the low momentum transfer $(|\mathbf{q}|<1$ a.u.$)$ $(e,3e)$ reaction [20]. In both these cases the four peaks emerge as "islands" between the nodal lines formed due to the dipole symmetry and the interelectron repulsion. For the equal-energy-sharing $(\gamma,2e)$ reaction all four peaks are identical in shape and magnitude. They correspond to both electrons leaving at about $\pm60°$ with respect to the polarization vector direction $\pm e$ and having a relative angle of $|\theta_b-\theta_c|\cong120°$. In the case of the low-q $(e,3e)$ reaction, due to the nonequivalence of the $\pm\mathbf{q}$ directions, the four peaks split into two pairs. Those two peaks in which both electrons leave at about $\pm60°$ with respect to the $+\mathbf{q}$ direction become more pronounced.

As the momentum transfer becomes large $(|\mathbf{q}|=2$ a.u. in the present case) the four-peak cross-section pattern undergoes a further transformation. The most prominent cross-section maximum (marked B in Fig. 3) corresponds to a configuration where one electron is emitted roughly in the direction of the momentum transfer $\mathbf{q}$ and the second one leaves in the opposite direction $-\mathbf{q}$ (back-to-back emission). This is the well-known configuration of collinear Wannier escape. In the $(\gamma,2e)$ reaction on ground-state He this escape is dominant in the vicinity of the ion core (the so-called Coulomb zone). However, outside the Coulomb zone the Wannier escape is suppressed due to the dipole selection rule [11,25]. As $|\mathbf{q}|$ becomes large, the dipole selection rule relaxes and Wannier escape becomes possible to the asymptotic region of large distances where it can be observed experimentally.

The second pair of peaks (A), which is of lower magnitude, is observed at about the same electron angles as the $+\mathbf{q}$ dipolelike peak in the low-q $(e,3e)$ reaction (i.e., for both electrons at angles of about $60°$ with the momentum transfer direction $\mathbf{q}$ and having a relative angle of $|\theta_b-\theta_c|\cong120°$). If the energies of the ejected electrons are increased the structure of the cross section is maintained but there is a profound
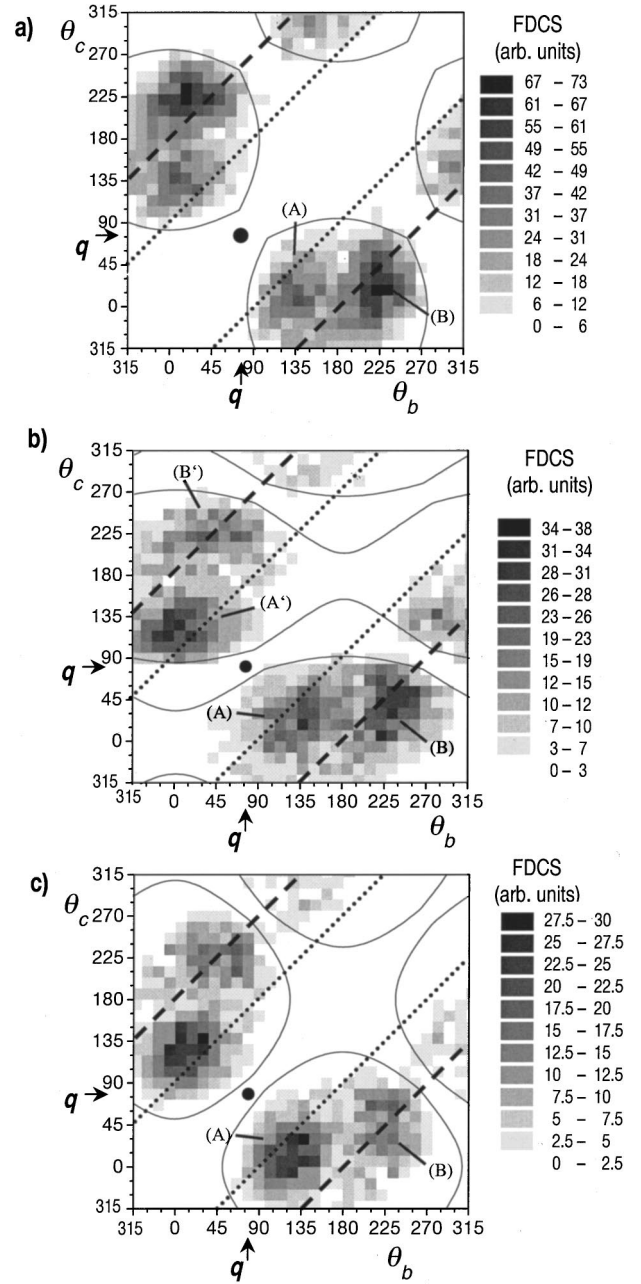

FIG. 3. Fivefold differential cross sections for $E_0=2$ keV and $|\mathbf{q}|=2$ a.u. in coplanar scattering geometry (see Fig. 2). In all diagrams dashed lines mark angular combinations for which the relative electron emission angle is $|\theta_b-\theta_c|=180°$ and dotted lines mark relative angles $|\theta_b-\theta_c|=90°$. The angular range inside the solid circular lines is not affected by the detector dead time. (a) Experimental cross section for $E_b=E_c=5$ eV. The direction of the momentum transfer $\mathbf{q}$ is marked by arrows and the solid circle in the diagram; its diameter indicates the experimental angular resolution. (b) $E_b=5$ eV and $E_c=25$ eV. (c) $E_b=E_c=20$ eV.

change of the relative magnitudes of the maxima. For asymmetric energy sharing with $E_b=5$ eV and $E_c=25$ eV [Fig. 3(b)] the reflection symmetry with respect to the line $\theta_b=\theta_c$ is broken. The peak B is most dominant, corresponding to the fast electron going to $\mathbf{q}$ and the slow electron being emitted in the opposite direction, while the reverse configu-

ration is relatively unimportant (peak B'). The peaks A and A' are still similar in magnitude and close in position to the $+\mathbf{q}$ dipolelike peaks. It should be mentioned that for this asymmetric-energy-sharing case cuts through the cross-section pattern exist that are not affected by the electron detector dead time. If the fast-electron angle is fixed to the forward or backward direction, the FDCS is obtained for scanning the slow electron over the full angular range from $0°$ to $360°$. Finally, if both electron energies are increased to $E_b = E_c = 20$ eV [Fig. 3(c)] back-to-back emission (peaks B) becomes relatively unimportant compared to emission of both target electrons into the half plane of the momentum transfer (peaks A).

In Fig. 4 theoretical cross sections are shown. The calculations were performed within the same model as employed in [12]. The interaction of the fast projectile with the target is described within the first Born approximation while the interaction of the slow ejected electrons is treated nonperturbatively using the convergent close-coupling method. This method is known to yield very reliable quantitative results for a related double-photoionization process when the two electrons are ejected from the helium atom by photon impact [24,26]. The helium ground state is described by a 20-parameter Hylleraas wave function. To test the sensitivity of the model to the ground state we performed some selected computations with a much simpler four-term multiconfiguration Hartree-Fock wave function. The difference between the two kind of calculation was only marginal. Therefore we conclude that the CCC model is not sensitive to the ground state for the present kinematics.

The calculations are in good agreement with the experimental data concerning the observed cross-section patterns and the evolution of the relative peak intensities in going from low energies via asymmetric energy sharing to higher energies $E_{b,c}$. The absolute magnitude of the cross section is not determined experimentally but the relative scale of the different cross sections shown in Fig. 3 is fixed. Theoretically, the equal-energy-sharing FDCS's are determined fully *ab initio* and can therefore be compared directly with the experimental results. The unequal-energy-sharing case is somewhat more tenuous. Due to unphysical oscillations in the energy-sharing distribution between the two ionized electrons, an accurate determination of the magnitude of the FDCS requires an additional rescaling procedure [27]. This procedure has been implemented for double-photoionization calculations [28] but not yet for $(e,3e)$. The theory reproduces the relative magnitudes fairly well for the equal-energy-sharing case, in particular concerning the heights of the peaks A in Figs. 3(a) and 3(c). However, the relative magnitude for the unequal-energy-sharing case in Fig. 4(b) is off by more than a factor of 2. This disagreement might be due to the above-mentioned oscillations in the energy-sharing distribution between the two ionized electrons, which can be remedied by an empirical rescaling procedure.

Another deviation that is significant within the present experimental statistics is a shift of the peaks B with respect to the experimental cross sections. The theoretical results, which are of first order in the projectile-target interaction, must show complete axial symmetry with respect to the mo-
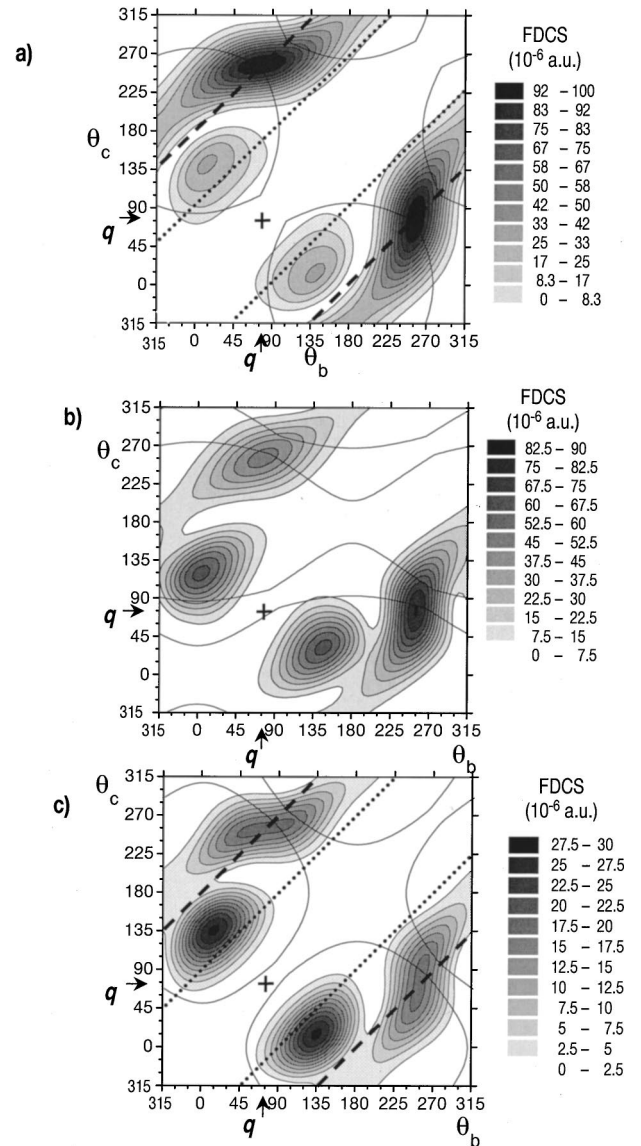

FIG. 4. Theoretical FDCS's for the same conditions as in Fig. 3 calculated using the convergent close-coupling method to treat the interaction of the slow ejected electrons nonperturbatively. The experimentally accessible angular range is indicated and lies within the solid circular lines (see also Fig. 3). (a) $E_b = E_c = 5$ eV. (b) $E_b = 5$ eV and $E_c = 25$ eV. (c) $E_b = E_c = 20$ eV.

mentum transfer direction. Therefore the cross section is invariant for reflection of both momentum vectors in the direction of $\mathbf{q}$. In the diagrams of Fig. 4 this corresponds to an inversion at the points where both electron emission angles are equal or opposite to the angle of $\mathbf{q}$ or at points where one angle is equal while the other is opposite to the angle of $\mathbf{q}$. The cross-section peak B of the theoretical result satisfies this symmetry. Its maximum occurs for a configuration where one electron leaves exactly parallel to $\mathbf{q}$ and the other is emitted perfectly opposite. In the experiment [Fig. 3(c)] the peak B is shifted along the dashed diagonal line to smaller angles for both electrons. Such a deviation from the axial symmetry with respect to $\mathbf{q}$ is a signature of second- or higher-order projectile-target interactions. This effect has
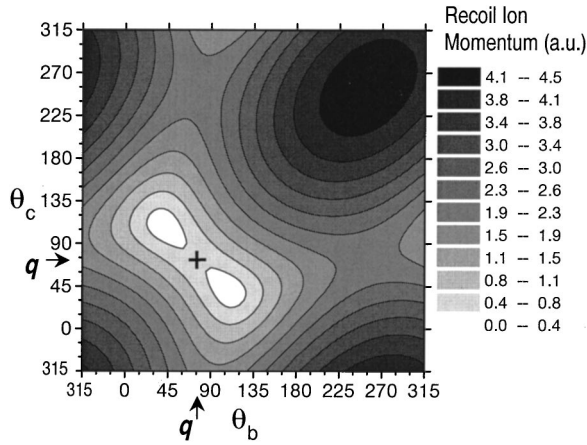
FIG. 5. Amount of recoil-ion momentum $|\mathbf{k}_{ion}| = |\mathbf{q} - \mathbf{k}_b - \mathbf{k}_c|$ as a function of the ejected-electron emission angles θ_b and θ_c ($|\mathbf{q}| = 2$ a.u.) for $E_b = E_c = 20$ eV.

been observed before for low-momentum-transfer collisions [20] and at energies as high as 5.5 keV [23]. Investigations of the total double-to-single ionization cross-section ratio also indicate that double collisions contribute for the present primary energy of 2 keV [29].

In order to understand the evolution of the relative strengths of the maxima *A* and *B* in Figs. 3(a)–3(c) (experiment) and 4(a)–4(c) (calculation) it is instructive to consider the magnitude of the recoil momentum of the ion in the final state $|\mathbf{k}_{He^{2+}}|$. The cross section for a clean binary knock-out collision should peak under the so-called Bethe kinematics where the recoil-ion momentum is small or vanishing. In Fig. 5 $|\mathbf{k}_{He^{2+}}|$ is given for $E_b = E_c = 20$ eV as a function of the electron emission angles θ_b and θ_c. In the whole range of angular combinations θ_b, θ_c there are two positions for which the recoil-ion momentum vanishes. These are configurations where both electrons are emitted symmetrically with respect to $\mathbf{q}$, each enclosing about a 40° angle with the momentum transfer direction and 80° with each other. The cross section in experiment [Fig. 3(c)] and theory [Fig. 4(c)] peaks for roughly these angular combinations. This proximity to the Bethe kinematics enhances the strength of the peaks *A*.

If the energy of the ejected electrons is lowered from 20 down to 5 eV the peaks *A* become relatively unimportant features compared to the peaks *B*. It must be pointed out that in this case the kinematics is not favorable for clean binary knock-out collisions since for all electron ejection angles the residual ion carries away a considerable momentum. The energies of the ejected electrons correspond to rather small momenta of $|\mathbf{k}_{b,c}| = 0.6$ a.u. and thus the Bethe condition $|\mathbf{k}_{ion}| \cong 0$, or with Eq. (1) $\mathbf{k}_b + \mathbf{k}_c \cong \mathbf{q}$, cannot be satisfied even if both electrons leave in the momentum transfer direction. So neither of the peaks *A* or *B* is favored by the Bethe kinematics.

At the same time, the growing strength of the peak *B* can be understood from the dominance of electron repulsion near the ionization threshold [30]. In a related $(e,2e)$ process at small excess energies over the threshold an enhanced back-to-back emission is observed with one electron going essentially to the forward and the other to the backward direction

with respect to the incoming beam. This is the collinear escape configuration which gives rise to the well-known Wannier threshold law. The recoiling ion carries the full momentum transfer, which is equal to the momentum of the incoming electron.

Concerning the ionization mechanisms responsible for peaks *A*, we can rule out the TS2 process. This is so because our measurement is in agreement with first-order CCC theory and demonstrates symmetry with respect to the **q** vector. Since it is not a single electron but the ejected electron pair which carries the momentum **q** transferred in the collision, the ionization must occur via electron correlation. Therefore we assign cross-section maxima *A* to the TS1 process, which is also consistent with the observed relative emission angle close to 90° and the small recoil-ion momentum. The very same TS1 process gives rise to a pair of dipolelike $+\mathbf{q}$ peaks in the low-q $(e,3e)$ reaction, which evolve into the peaks *A* under the present kinematical condition of a large momentum transfer. We note that there is no counterpart to the Wannier-like peaks *B* in either the $(\gamma,2e)$ reaction or the low-q $(e,3e)$ reaction since the Wannier escape is strongly suppressed by the dipole symmetry.

As to another possible mechanism of double ionization, the shake-off process, we rule out it playing an important role under the present kinematical conditions. In principle, it can give rise to an emission configuration similar to the peak *B* with one electron that is ionized in a direct knockout going roughly along **q**. The angular distribution of the second or "shake-off" electron is not necessarily isotropic but due to the final-state repulsion it is preferentially emitted in the opposite direction. The typical shake-off emission characteristics are displayed in the unequal-energy-sharing case illustrated in Fig. 3(b). Here peak *B* corresponds to the fast electron ($E_c = 25$ eV) moving along **q** and the slow electron ($E_b = 5$ eV) moving in the opposite direction. On the other hand, for the shake-off to take place, a sudden change of the atomic potential is required. So the wave function of the residual electron cannot adapt adiabatically to the ionic potential. Therefore the velocity of the electron that is knocked out in a binary collision should be considerably higher than the classical orbital velocity of the remaining bound target electron. Since this is not the case for the present experiment we conclude that the cross sections presented here are consistent with the TS1 process except for minor contributions of higher order for peak *B*.

Finally, we study the cross sections for a case of noncoplanar scattering geometry. As illustrated in Fig. 6, we have chosen one electron to be emitted 45° above the scattering plane ($\phi_b = 45°$) and the second going 45° below the scattering plane ($\phi_c = 135°$) with energies $E_{b,c} = 20$ eV. This geometry was used by Ford *et al.* [16] for the $(e,3e)$ reaction on the magnesium atom. The authors' intention was to obtain the two-electron momentum density in analogy to the one-electron momentum density measured with electron momentum spectroscopy (EMS) using a binary $(e,2e)$ reaction. Only recently has the experimental observation of an atomic two-electron momentum distribution been reported [18].
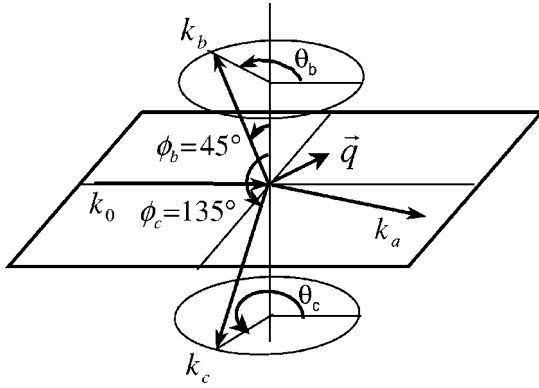
FIG. 6. A particular case of noncoplanar scattering geometry. The polar angles are chosen to be $\phi_b = 45°$ and $\phi_c = 135°$.

As in the case of the coplanar kinematics, the out-of-plane experimental [Fig. 7(a)] and theoretical cross sections [Fig. 7(b)] agree very well. For this kinematics the electron momentum sum $\mathbf{k}_b + \mathbf{k}_c$ always lies in the scattering plane. It is directed parallel to $\mathbf{q}$ if the momentum transfer axis is in the plane spanned by $\mathbf{k}_b$ and $\mathbf{k}_c$ or $(\theta_b - \theta_q) + (\theta_c - \theta_q) = 0$. This condition is satisfied along the dashed lines in Fig. 7 where
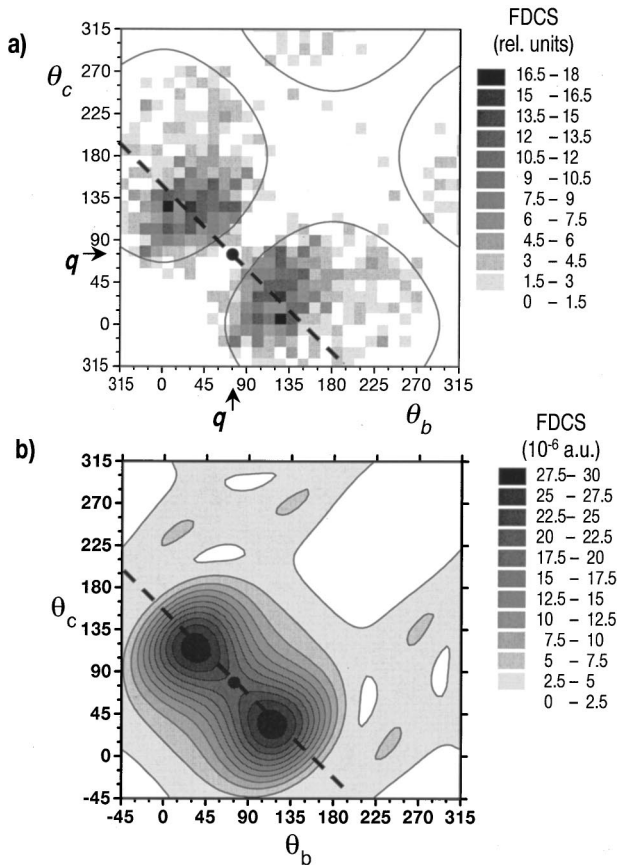

FIG. 7. Fivefold differential cross section for the out-of-plane geometry given in Fig. 6. (a) Experiment. The momentum transfer is $|\mathbf{q}| = 2.0 \pm 0.4$ a.u. and the electron energies are $E_b = E_c = 20$ eV. (b) CCC theory. The dashed lines mark angular combinations for which the electron momentum sum is parallel to the momentum transfer direction $(\mathbf{k}_b + \mathbf{k}_c) \| \mathbf{q}$.

we see two binary peaks in the cross sections. The recoil-ion momentum is minimal if the azimuthal angles of both electrons are equal to the momentum transfer direction $\theta_b = \theta_c = \theta_q$. While in the experiment this angular combination is not accessible because of the detector dead time, the theory shows a rather large cross section at this point (marked by a dot). This reflects the reduced electron repulsion in the present out-of-plane geometry compared to the coplanar geometry since both electrons still enclose the relative angle $\phi_c - \phi_b = 90°$. The cross section peaks for angles θ_b, θ_c that are about $40°$ off θ_q and therefore allow for lower electron repulsion between the ejected electrons.

It is instructive to follow the evolution of the cross-section pattern in the present out-of-plane geometry in going from the (γ,2e) reaction to the low-q (e,3e) reaction and finally arriving at the present high-q (e,3e) reaction. Although the experimental data are not available for such an analysis, the numerical simulation can easily be performed. In the out-of-plane (γ,2e) reaction the cross-section pattern consists of two pairs of equivalent maxima squeezed by rigid nodal lines due to the dipole symmetry. As the interelectron repulsion is significantly weakened for the out-of-plane geometry, the corresponding nodal line $\theta_b = \theta_c$ is reduced to a shallow valley, and the two neighboring peaks in the pair merge together. The same pattern remains for the low-q (e,3e) reaction with two stronger maxima in which the electrons escape closer to the $+\mathbf{q}$ direction and two weaker maxima for the opposite $-\mathbf{q}$ escape direction. At large $|\mathbf{q}|$ the Bethe condition can be satisfied in the proximity of the $+\mathbf{q}$ peaks and they become the only prominent feature of the cross-section pattern as is seen in Fig. 7.

The second cross-section maximum B of the Wannier-like escape, which is present in the coplanar geometry and which shows signatures of higher-order contributions, is not present in this geometry. This confirms that the noncoplanar geometry was rightly chosen by Ford *et al.* to highlight first-order binary knock-out processes where the residual ion carries very little momentum. As to the present experimental arrangement, we are not able to perform EMS studies where the observed cross section reflects the two-electron momentum distribution in the initial target state. This is because the final-state interaction of the ejected electrons cannot be made negligible for low emission energies of $E_{b,c} = 20$ eV.

IV. SUMMARY

We have presented experimental and theoretical fully differential cross sections for double ionization of helium by 2-keV electron impact. The measurements were performed employing our reaction microscope which allows us to detect simultaneously a large part of the final-state momentum space. These cross sections, obtained in the conventional angle-scanning mode, could therefore be presented as three-dimensional plots for a large range of the electron emission angles θ_b and θ_c. This allows us to identify easily the symmetries and characteristics of the cross sections and to compare them with the results of calculations. Furthermore, the large momentum-space acceptance enabled a systematic investigation of the double-ionization dynamics for different kinematical conditions, i.e., different energies for the ejected

electrons and the coplanar and out-of-plane scattering geometry. The restrictions on the accessible angular range imposed by the electron detector dead time are mainly in an angular range where the cross section is small due to electron repulsion in the final state.

For the present case of a large momentum transfer the cross-section pattern is formed by two pairs of well-defined maxima characterized by the ejected-electron emission angles $\theta_{b,c}$. One pair of maxima (marked in the figures as A) dominates the cross-section pattern for higher energies of the ejected electrons in the kinematics that satisfies the Bethe ridge condition $|\mathbf{k}_{ion}| \cong 0$. It is tempting to call these maxima binary as they are strongly enhanced under the binary knock-out Bethe ridge condition, especially in the out-of-plane kinematics. However, very similar peaks, albeit not so prominent, are seen in the low-q or/and low-E $(e,3e)$ reactions and the $(\gamma,2e)$ reaction far away from the Bethe ridge. This observation can be explained by the dipole symmetry rules which still play some role in forming the peaks A even at large momentum transfer.

In the "binary" peaks A the most probable relative electron angle is close to 90° and within the present statistics the cross section is symmetric with respect to the momentum transfer direction. These observations are signatures that the TS1 mechanism is responsible for the double-ionization process. We drew a similar conclusion in a previous experiment at 3-keV electron impact [19] for cross sections differential with respect to the relative emission angle of the ejected electrons only: The most probable relative emission angle, which peaks at 145° for the dipole limit, comes close to 90° for the conditions of a large momentum transfer and a small recoil-ion momentum.

A second pair of peaks in the cross section (marked B) corresponds to the Wannier configuration with the two electrons emitted back to back, which is the most favored configuration for two outgoing electrons with small excess energy. There is no counterpart of the peaks B in either the $(\gamma,2e)$ or the low-q $(e,3e)$ reaction on ground-state He, since the Wannier escape is strongly suppressed by the dipole symmetry. In the present high-q $(e,3e)$ reaction, higher-multipole transitions contribute to this escape configuration.

We attribute the origin of both the peaks A and B to the TS1 double-ionization mechanism. This is confirmed by the generally good agreement between the present experimental results and calculations performed within the CCC model which treats the projectile-target interaction to first order. However, the observed shift of the peaks B with respect to the momentum transfer direction (not seen in the calculation) indicates that higher-order projectile-target interactions also make some contribution.

Finally, we have presented data for a noncoplanar geometry where one electron is emitted 45° above and the second electron 45° below the scattering plane. In this geometry the double-ionization processes occurs with the ion left with a low recoil momentum. It is therefore ideally suited to restrict the double-ionization mechanism to a direct knockout of both target electrons without participation of the nucleus.

[1] H. Ehrhardt, M. Schulz, T. Tekaat, and K. Willmann, Phys. Rev. Lett. **22**, 89 (1969).

[2] U. Amaldi, Jr., A. Egidi, R. Marconero, and G. Pizzella, Rev. Sci. Instrum. **40**, 1001 (1969).

[3] C. T. Whelan, Science **286**, 2457 (1999).

[4] T. N. Rescigno, M. Baertschy, W. A. Isaacs, and C. W. McCurdy, Science **286**, 2474 (1999).

[5] M. Brauner, J. S. Briggs, and H. Klar, J. Phys. B **22**, 2265 (1989).

[6] J. Berakdar, Phys. Rev. A **53**, 2314 (1996).

[7] S. P. Lucey, J. Rasch, and C. T. Whelan, Proc. R. Soc. London, Ser. A **455**, 349 (1999).

[8] J. Berakdar, Phys. Rev. A **54**, 1994 (1997).

[9] A. W. Malcherek and J. S. Briggs, J. Phys. B **30**, 4419 (1997).

[10] A. Lahmam-Bennani, I. Taouil, A. Duguet, M. Lecas, L. Avaldi, and J. Berakdar, Phys. Rev. A **59**, 3548 (1999).

[11] J. Berakdar and H. Klar, J. Phys. B **26**, 4219 (1993).

[12] A. Kheifets, I. Bray, A. Lahmam-Bennani, A. Duguet, and I. Taouil, J. Phys. B **32**, 5047 (1999).

[13] M. Grin, C. Dal Capello, R. El Mkhanter, and J. Rasch, J. Phys. B **33**, 131 (2000).

[14] A. Lahmam-Bennani, C. Dupré, and A. Duguet, Phys. Rev. Lett. **63**, 1582 (1989).

[15] A. Duguet, A. Lahmam-Bennani, M. Lecas, and B. El Marji, Rev. Sci. Instrum. **69**, 3524 (1998).

[16] M. J. Ford, J. P. Doering, J. H. Moore, and M. A. Coplan, Rev. Sci. Instrum. **66**, 3137 (1995).

[17] I. Taouil, A. Lahham-Bennani, A. Duguet, and L. Avaldi, Phys. Rev. Lett. **81**, 4600 (1998).

[18] B. El Marji, J. P. Doering, M. A. Coplan, and J. H. Moore, Phys. Rev. Lett. **83**, 1574 (1999).

[19] A. Dorn, R. Moshammer, C. D. Schröter, T. J. M. Zouros, W. Schmitt, H. Kollmus, R. Mann, and J. Ullrich, Phys. Rev. Lett. **82**, 2496 (1999).

[20] A. Dorn, A. Kheifets, C. D. Schröter, B. Najjari, C. Höhr, R. Moshammer, and J. Ullrich, Phys. Rev. Lett. **86**, 3755 (2001).

[21] R. Moshammer *et al.*, Nucl. Instrum. Methods Phys. Res. B **108**, 425 (1996); H. Kollmus *et al.*, *ibid.* **124**, 377 (1997).

[22] T. A. Carlson and M. O. Krause, Phys. Rev. **140**, 1057 (1965).

[23] B. El Marji, C. D. Schröter, A. Duguet, A. Lahmam-Bennani, M. Lecas, and L. Spielberger, J. Phys. B **30**, 3677 (1997).

[24] A. S. Kheifets and I. Bray, J. Phys. B **31**, 5149 (1998).

[25] F. Maulbetsch and J. S. Briggs, J. Phys. B **24**, 1917 (1993).

[26] A. S. Kheifets and I. Bray, Phys. Rev. Lett. **81**, 4588 (1998).

[27] I. Bray, Phys. Rev. Lett. **78**, 4721 (1997).

[28] A. Kheifets and I. Bray, J. Phys. B **31**, L447 (1998).

[29] J. H. McGuire, Phys. Rev. Lett. **49**, 1153 (1982).

[30] M. Brauner, J. S. Briggs, H. Klar, J. T. Broad, T. Rösel, K. Jung, and H. Ehrhardt, J. Phys. B **24**, 657 (1990).